Available online at www.sciencedirect.com
SCIENCE DIRECT®
Journal of Nuclear Materials 353 (2006) 167–176
journal of nuclear materials
www.elsevier.com/locate/jnucmat

Characterization of hydrogen concentration in Zircaloy-4 using ultrasonic techniques

M.P. Gómez [a,b,*], G. Domizzi [c], M.I. López Pumarega [d], J.E. Ruzzante [b,d]

[a] *Department of Electronic Engineering, Facultad Regional Buenos Aires, Universidad Tecnológica Nacional, Medrano 951 (C1179AAQ) Buenos Aires, Argentina*
[b] *Institute of Technology 'Prof. Jorge Sábato', Universidad Nacional de General San Martín, Av. Gral. Paz 1499 (B1650KNA) San Martín, Buenos Aires, Argentina*
[c] *Materials Department, Centro Atómico Constituyentes, Comisión Nacional de Energía Atómica, Av. Gral. Paz 1499 (B1650KNA) San Martín, Buenos Aires, Argentina*
[d] *Non-Destructive and Structural Testing Department, Centro Atómico Constituyentes, Comisión Nacional de Energía Atómica, Av. Gral. Paz 1499 (B1650KNA) San Martín, Buenos Aires, Argentina*

Received 4 October 2005; accepted 24 January 2006

Abstract

The relationship between hydrogen concentration precipitated as hydride particles and ultrasonic parameters, such as velocity and attenuation, was examined in Zircaloy-4 samples for potential applications in the Non-Destructive Test Field. Different amounts of hydrogen (up to 517 ppm) were introduced in the samples by gaseous charging. Ultrasonic attenuation measurements were performed with compressive waves at frequencies of 10 and 30 MHz, and propagation velocity measurements were performed at 10 MHz. Ultrasonic velocity showed an approximately linear increase with hydrogen concentration and it could be used as an assessment parameter when the hydrogen level is high enough. Attenuation versus hydrogen concentration has been fitted by a logarithmic equation at 10 MHz. At 30 MHz a fluctuating behavior of the attenuation prevented measurement of the hydrogen concentration.

PACS: 81.70; 43.35; 61.82.Bg

1. Introduction

Zirconium alloys are the selected materials for the production of main components in nuclear reactors. For example, pressure tubes of CANDU reactors are made of Zr–2.5Nb and Zircaloy-2 while Zircaloy-4 is the alloy used for fuel cladding tubes. Their advantages are the very low neutron absorption cross-section, adequate mechanical

* Corresponding author. Address: Department of Electronic Engineering, Facultad Regional Buenos Aires, Universidad Tecnológica Nacional, Medrano 951 (C1179AAQ) Buenos Aires, Argentina. Tel.: +54 11 6772 7235; fax: +54 11 6772 7355.
E-mail address: mpgomez@cnea.gov.ar (M.P. Gómez).

0022-3115/$ - see front matter © 2006 Elsevier B.V. All rights reserved.
doi:10.1016/j.jnucmat.2006.01.024

properties and good corrosion resistance [1]. Nevertheless, nuclear components are exposed to severe conditions such as corrosion at high temperatures and pressures, and high radiation levels. Initial hydrogen concentration is nearly 20 ppm in weight but, during service, this value increases by several factors such as: corrosion reactions, water hydrolysis and others due to the reactor environment [2]. The hydrogen fraction absorbed by the material (pick up), depends on the alloy, the kind of formed oxide, and the radiation level [3]. Under these conditions, when hydrogen solid solubility is surpassed, zirconium hydride particles precipitate, resulting in mechanical properties degradation of material [4]. Examples of this are cracking of pressure tubes (Zircaloy-2 and Zr–2.5Nb) caused by blisters [5,6], cracking in cladding tubes (Zircaloy-4) [7,8], and other phenomena such as delayed hydride cracking in the presence of a stress gradient [9].

At present, there is no 'non-destructive method' to evaluate precipitated hydride quantities in Zr-alloys. This evaluation would be very useful for life prediction of nuclear components in service. For this reason it is important to assess different non-destructive techniques in order to find the one that allows to solve that challenge. De et al. [10] performed an exhaustive analysis using different non-destructive techniques for hydride assessment in Zircaloy-2. These authors studied the ultrasonic propagation of longitudinal and transverse waves at different frequencies, in samples hydrided by high temperature autoclaving. They showed a fluctuating behavior of the velocity as hydrogen level increases. They justified this fact by the change in the ratio of γ and δ hydrides quantities. When hydrogen concentration increases, hydrides alter their morphology and this fact introduces some amount of strain in the lattice. The density and elastic modulus of γ and δ hydrides are different, and lower than that of α-Zr. Thus, they concluded that the velocity may vary depending on the hydride distribution.

The aim of this work is to continue the analysis about the feasibility of hydrides quantification by means of ultrasonic measurements (with pulse echo technique). For this reason, the propagation velocity and the attenuation of longitudinal waves were studied for Zircaloy-4 hydrided by the gaseous charge method.

This is a preliminary study to evaluate the scope of this technique. In the future, another sensors and configurations must be tested to be employed in nuclear components.

2. Experimental procedure

2.1. Specimen preparation

Samples were cut from a cold rolled and annealed (700 °C) Wah Chang Albany Zircaloy-4 bar, with 23 mm × 10 mm squared section. Its composition was Sn 1.55, Fe 0.21, Cr 0.11, O 1180 ppm (mg/kg). The initial hydrogen concentration (C_0) was specified in (15 ± 5) ppm. The microstructure, as corroborated by metallography (see Fig. 1), consisted of equiaxed grains uniformly distributed. The measured ASTM grain size was approximately 10 (11 μm).

The sample dimensions were 27.0 mm × 23.0 mm × 6.4 mm. Ten samples, labeled H1–H10, were individually hydrided in a gaseous charge device outlined in Fig. 2. The original hydrogen concentration was increased in the range 14–517 ppm in weight. Three samples, labeled N1–N3, were not hydrided. Sample N1 was used as a standard of the as-received material; N2 and N3 had the same thermal treatment than the hydrided samples, to corroborate that the hydriding process did not introduce changes at the microstructure.

Previous to the hydriding charge, the samples were coated with an electrodeposited palladium film, in order to promote the hydrogen uptake during charge, by avoiding the surface oxidation of Zircaloy-4. Edges of samples were ground in order to eliminate the Pd film, so the hydrogen entered only through faces of the sample and thus the finally obtained hydride distribution was more uniform. The chamber containing the sample was evacuated (5×10^{-3} Pa), and it was heated up to (270 ± 10) °C under dynamic vacuum. Then, the chamber was closed and a known quantity of hydrogen was introduced. After hydrogen absorption, the sample

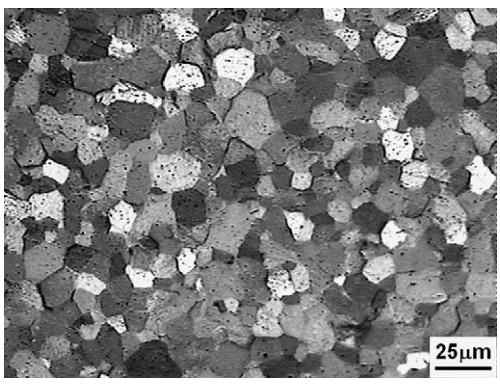

Fig. 1. Microstructure of the as received material.

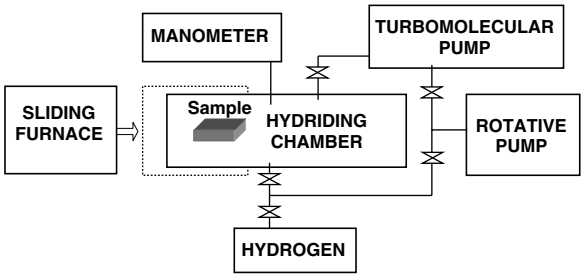

Fig. 2. Hydriding device.

was cooled down to room temperature. The hydrogen concentration in the sample was calculated from the difference between the initial and final pressure measured at room temperature assuming ideal gas behavior. The error was less than 4.5%. This calculation was corroborated by the sample weight increase. Then, each sample was again introduced into the chamber and hydrogen pressure was increased up to 10^5 Pa, at room temperature. This produced the hydriding of the Pd film and promoted its detachment from the Zircaloy-4 sample. During charging a hydride layer was formed on the sample surface. In order to obtain a uniform hydride distribution throughout the sample, a homogenization heat treatment was applied. H–Zr equilibrium diagram presents a eutectoid transformation at ≈550 °C. To avoid both, phase transformation and the alteration of the original microstructure of samples the homogenization temperature was lower than 550 °C and higher than the dissolution temperature [11]. The heat treatment was long enough to produce diffusion through the sample thickness [12]. Samples H1–H8 were heat treated at (410 ± 10) °C, samples N2 and H9 at (537 ± 5) °C and samples N3 and H3 at (543 ± 5) °C. Samples N2 and N3 were not hydrided and were used to corroborate that the heat treatments did not alter the microstructure characteristics of the 'as-received' material. Homogenization heat treatments were performed under static vacuum conditions in order to induce the deposition of a thin oxide film on the Zircaloy surface and prevent the sample dehydriding. After homogenization, the oxide film was removed. Each sample was ground using a device that guarantees parallelism between its faces and reduced the thickness down to 5.92 mm, with an error lower than 0.01 mm.

2.2. XRD and metallographic analysis

Four representative samples (N1, H3, H7 and H10) were analyzed, on the rolling plane, by means of X-ray diffraction (XRD) techniques in order to characterize hydrides.

The equipment and settings used were the following:

Philips PW3710 Analytical Based Diffractometer.
PC-APD, diffraction software.
Cu K_α radiation.
Scan step size = 0.020° and 0.030°.
No monochromator used.

For XRD, the surfaces of the samples were ground with emery paper down to 2500 mesh, and they were polished with ammonium dichromate ash. All samples were polished and etched, on the transverse section, with a solution of: nitric acid 45 ml, lactic acid 45 ml and hydrofluoric acid 4 ml. Then, they were observed by optical microscopy to corroborate that hydride distribution was homogeneous.

2.3. Ultrasonic measurement

For ultrasonic measurements the following equipment and products were used:

- MATEC 7700 Emitter–Receiver Module.
- MATEC 760 Oscillator (10–90 MHz range).
- MATEC 110 and 122B External Synchronism Module.
- LeCroy 9360 Digital Oscilloscope (600 MHz, 5 Gigasamples/s).
- Compaq Presario Notebook.
- Scope Explorer LeCroy software.
- Valpey–Fisher 10 MHz overtone 'X-cut' quartz transducer.
- Ultragel couplant.

The ultrasonic system (Fig. 3) was assembled for pulse-echo technique in direct coupling [13]. A controlled in length, frequency and amplitude electric pulse generated by the emitter–receiver system (Matec 7700, 760, 110 and 122B modules) is converted to elastic waves by a 10 MHz quartz transducer. The ultrasonic pulse travels through the thickness of the sample, producing multiple reflections between its parallel faces. The echoes are converted in an electric signal by the same transducer. The emitter–receiver system receives and amplifies the signal, which is measured and digitized by a digital oscilloscope. The signals are transferred to a computer via a RS-232 communication device. A

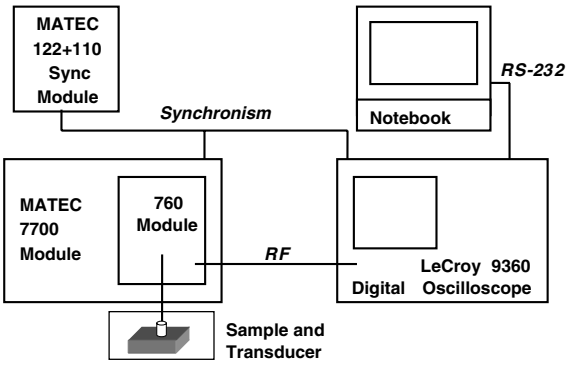

Fig. 3. Ultrasonic system.

signal of decaying echoes corresponding to the successive reflections is obtained.

Attenuation measurements were made by fitting an exponential curve to the decreasing back wall reflections and choosing the coefficient of the exponential to produce the best fitting.

Ultrasonic velocity measurements were performed by time of flight evaluation of the pulses across the sample. 'Overlap' [14] and 'Cross Correlation' [15] methods were used, obtaining similar results.

Measurement errors were analyzed for ultrasonic attenuation and velocity. The most relevant error sources for ultrasonic attenuation measurements were produced by the calibration of the ultrasonic emitter–receiver system, the spread of the ultrasonic beam generated by the transducer, spurious effects in the ultrasonic signal (by non-parallelism), and bonding of the transducer to the sample. To reduce the errors caused by system calibration, a specified frequency was adjusted in the emitter control panel, and all the samples were successively measured. This procedure produced a systematic error. A similar analysis can be made about the beam spread. It depends on the sensor diameter and wavelength of the ultrasonic wave. As the sensor diameter was constant and the wavelength nearly constant, the error introduced by the beam spread may be considered as a systematic one, which does not affect the qualitative behavior of the curves. The non-parallelism effects were reduced by means of a carefully ground of the samples. The transducer bonding error was experimentally evaluated and it was of ten percent of the measured value, approximately.

Time resolution of the digital scope and sample thickness measurement were the highest error sources in velocity measurement. Both factors were used to calculate the velocity error by error propagation. In this case, other sources of error such as those mentioned for attenuation can be considered negligible. Dispersion of waves and change of pulse shape due to attenuation of high frequency components in the sample had a very low effect over velocity error. This was corroborated by a Wavelet Transform analysis [16] applied to multiple echoes. Gabor wavelets showed that the ultrasonic energy was localized in a regular distribution of packets in the time-frequency spectrum.

3. Results and discussion

3.1. XRD results

N1, H3, H7 and H10 samples were evaluated with this technique. X-ray diffractograms showed the presence of δ-hydrides but no evidence of γ-hydrides was detected (Fig. 4). These results agree with those reported in literature [17]. The intensity of (1 1 1) δ-hydride line is weak in the non-charged sample and increases with hydrogen concentration.

3.2. Optical metallography

Fig. 5 shows optical micrographs with low and high magnification for samples N1, H3, H7 and H10. Hydride distribution homogeneity was evaluated at low magnification for all samples. The shape of hydride particles, observed at high magnification, corresponds to plate like precipitates.

3.3. Ultrasonic velocity measurement

Ultrasonic velocity was determined for longitudinal 10 MHz waves, in Zircaloy-4 hydrided samples. Table 1 shows the velocity and the added hydrogen quantity (in ppm) for each sample.

If ultrasonic velocity versus hydrogen concentration is displayed in a graph (Fig. 6), a smooth fluctuation can be observed for hydrogen concentration lower than 200 ppm. Measurement errors could be an explanation for this behavior, because the observed fluctuations are inside the error band. But in spite of these fluctuations, the experimental data for ultrasonic velocity can be fitted as showed in Fig. 6 as a function of the hydrogen concentration (C_H) by a linear regression:

$$V\ (\mathrm{m/s}) = a \times C_H\ (\mathrm{ppm}) + b, \qquad (1)$$

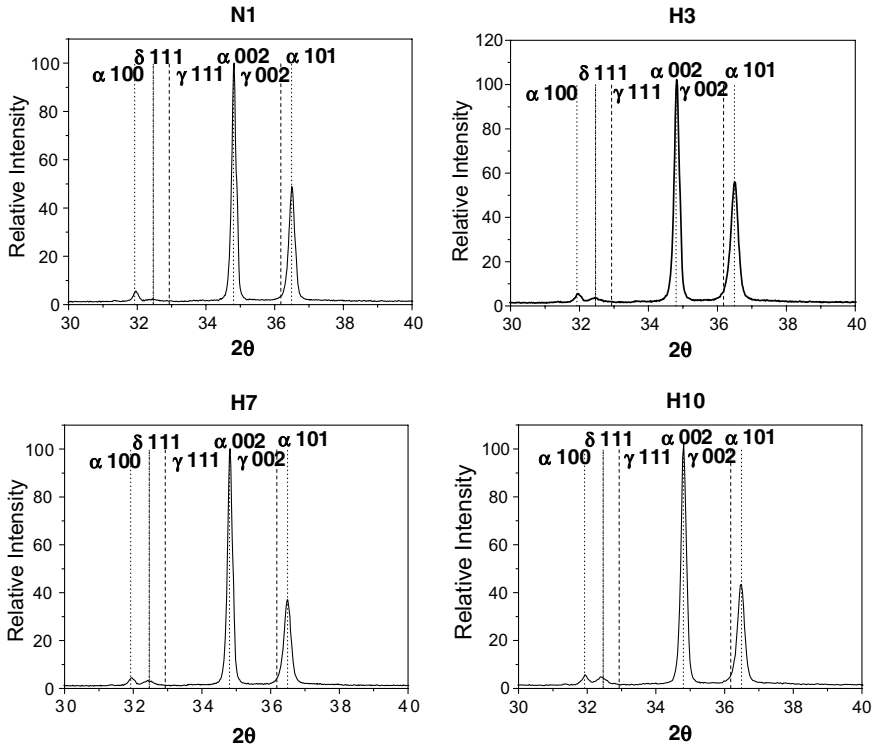

Fig. 4. X-ray diffractograms of Zircaloy-4 samples N1, H3, H7, H10.

where $a = 5.05 \times 10^{-2}$ and $b = 4634.9$, with a correlation coefficient $R = 0.98$ and an standard deviation SD = 1.6 m/s. The velocity error $\Delta V = 3.5$ is lower than 0.1% of the measured value. However the slope of the linear regression is smooth enough to produce an error in hydrogen concentration of $\Delta C_H = \Delta V/a = 60$ ppm. So, the relative error of this method is lower for higher hydrogen concentration. Then, Eq. (1) can be used to infer the hydrogen concentration by means of ultrasonic measurements, for a uniform hydride distribution, but this method is not enough sensitive to detect hydrogen concentration differences lower than 60 ppm. Besides, having into account the measurement errors, the fluctuating behavior reported by De et al. [10] could not be corroborated.

This method could be useful to detect high localized hydrogen concentration immersed in a low hydrogen concentration matrix, such as incipient hydride blisters, but more work must be done on this subject in the future.

The propagation velocity of elastic waves is proportional to the square root of the ratio of Young modulus (E) to density (ρ). The change in both parameters with increasing hydrogen concentration could explain the velocity behavior. Aladjem [18] reported that there is a fairly regular decrease in density with increasing hydrogen concentration from zero to 61.5 at.% (δ phase) in Zr alloys. The same behavior is observed in presence of γ-phase ZrH; however some difficulties in measurements made the reported values approximated. Table 2 shows values of density and elastic modulus reported in literature. The ratio E/ρ of zirconium hydride is lower than that of zirconium when the values reported by Beck and Mueller [19] are employed. This effect was argued by De et al. [10] to explain the reduction in velocity detected for hydrogen levels lower than 100 ppm in presence of γ phase. Nevertheless, more recently, Yamanaka et al. [20,21] found that for δ hydride the ratio E/ρ is higher than that corresponding to the Zr matrix. In the present paper only δ precipitates were detected by X-ray diffraction. Then, the increase of velocity with hydrogen concentration may be explained by the higher ratio E/ρ of the δ-hydride. The non-existence of γ hydrides implies that a competition phenomenon between δ and γ hydrides, as

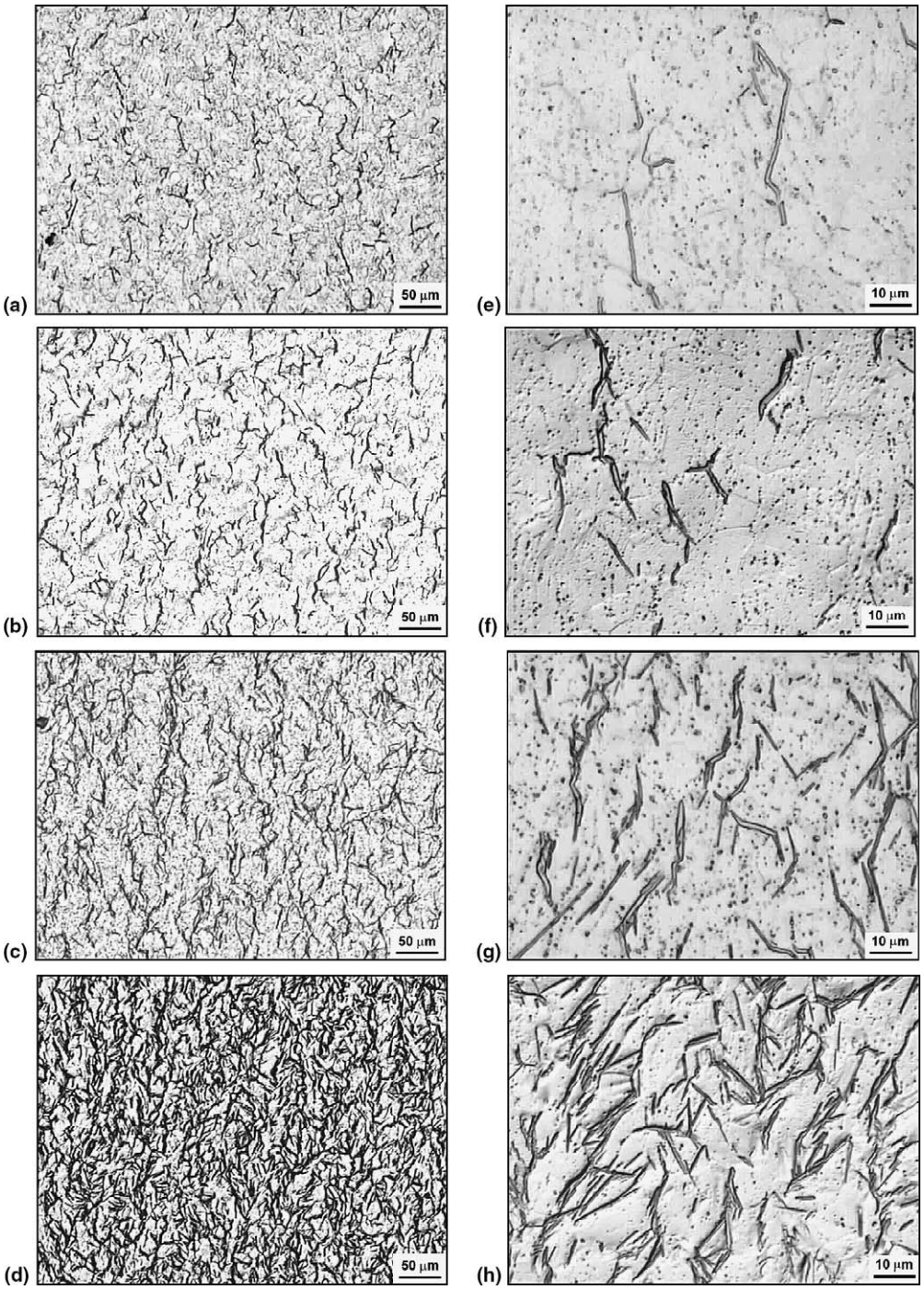

Fig. 5. Optical micrograph of Zircaloy-4 with different hydrogen concentration. Low magnification: (a) 75.5 wt ppm, (b) 185.6 wt ppm, (c) 319.5 wt ppm, (d) 531.7 wt ppm. High magnification: (e) 75.5 wt ppm, (f) 185.6 wt ppm, (g) 319.5 wt ppm, (h) 531.7 wt ppm.

described by De et al. [10], does not appear in the present work.

Results of the longitudinal waves velocity for the as-received material obtained for Zircaloy-4 in this work do not agree with those reported for Zircaloy-2 by De et al. [10]. An explanation, beyond the different materials, may be based on the work of Konishi and Honji [22] who performed measure-

Table 1
Measured velocity for Zircaloy-4 charged samples

Sample	Added hydrogen (ppm)	Velocity (m/s)
N1	0	4635.7 ± 3.5
N2	0	4635.7 ± 3.5
N3	0	4635.7 ± 3.5
H1	13.6 ± 0.6	4633.1 ± 3.5
H2	31.5 ± 1.4	4635.7 ± 3.5
H3	60.5 ± 2.7	4636.4 ± 3.5
H4	88.9 ± 4.0	4641.7 ± 3.5
H5	107.0 ± 4.8	4643.1 ± 3.5
H6	140.4 ± 6.3	4641.6 ± 3.5
H7	170.6 ± 7.7	4642.4 ± 3.5
H8	199.7 ± 9.0	4643.1 ± 3.5
H9	304.5 ± 13.7	4650.4 ± 3.5
H10	516.7 ± 23.3	4661.4 ± 3.5

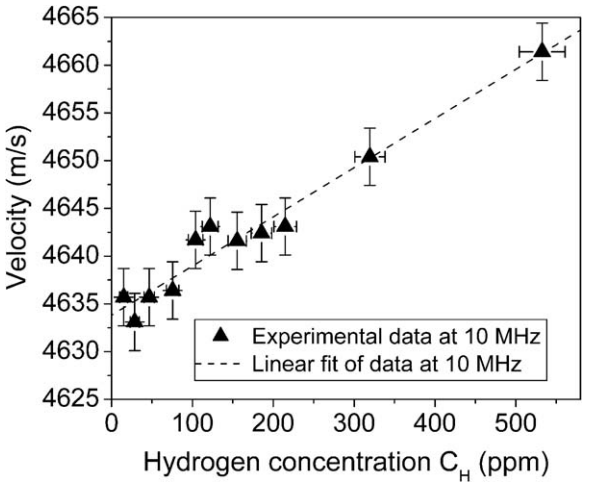

Fig. 6. Ultrasonic velocity versus hydrogen concentration.

Table 2
Density and elastic modulus for α-Zr, δ-Zr and γ-Zr

		α-Zr	γ-ZrH	δ-ZrH
Beck and Mueller [19]	Density ρ (g/cm^3)	6.5	5.84	5.65
	Elastic modulus E (GPa)	98.6	84.5	83.1
	Ratio E/ρ (GPa g/cm^3)	15.07	14.47	14.7
Yamanaka et al. [20,21]	Density ρ (g/cm^3)	6.5	–	5.65
	Elastic Modulus E (GPa)	95.5	–	131.7
	Ratio E/ρ (GPa g/cm^3)	14.67	–	23.3

ments in Zircaloy samples with different textures and metallurgical conditions. The texture influence on velocity was reflected in a spread of velocity values for the same material in the range between

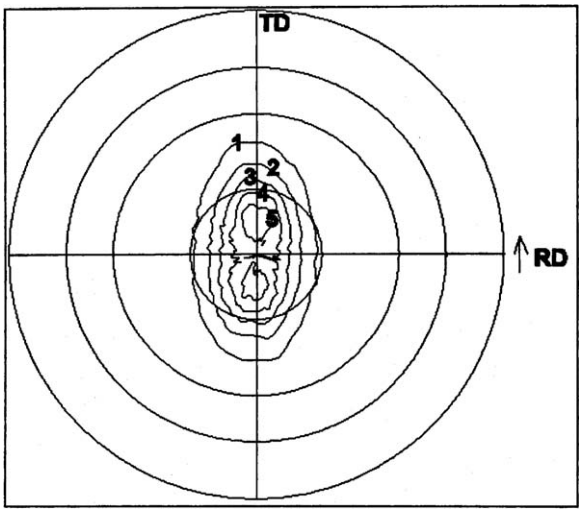

Fig. 7. Basal pole figure.

4650 m/s and 4850 m/s depending on the f-factor (the effective number of crystallites with the basal pole aligned with the direction perpendicular to the sample surface). In this work, the f-factor (or Kearns factor) was calculated for a sample in the as received condition and a value of 0.5 was obtained. The calculation was made with data extracted from the (0002) pole figure (Fig. 7) measured using an X-ray diffractometer.

3.4. Ultrasonic attenuation measurement

Attenuation versus added hydrogen for tested samples at 10 and 30 MHz is shown in Table 3 and 4, respectively. R^2 is the fitting coefficient of

Table 3
Attenuation coefficient α and R^2 fitting coefficient for Zircaloy-4 charged samples at 10 MHz

Sample	Added hydrogen (ppm)	R^2	Attenuation coefficient α (dB/cm)
N1	0	0.993	0.43 ± 0.04
N2	0	0.984	0.43 ± 0.04
N3	0	0.973	0.42 ± 0.04
H1	13.6 ± 0.7	0.991	0,50 ± 0.05
H2	31.5 ± 1.4	0.989	0.50 ± 0.05
H3	60.5 ± 2.7	0.991	0.56 ± 0.06
H4	88.9 ± 4.0	0.994	0.54 ± 0.05
H5	107.0 ± 4.8	0.997	0.59 ± 0.06
H6	140.4 ± 6.3	0.996	0.59 ± 0.06
H7	170.6 ± 7.7	0.960	0.61 ± 0.06
H8	199.7 ± 9.0	0.990	0.62 ± 0.06
H9	304.5 ± 13.7	0.966	0.65 ± 0.07
H10	516.7 ± 23.3	0.994	0.67 ± 0.07

Table 4
Attenuation coefficient α and R^2 fitting coefficient for Zircaloy-4 charged samples at 30 MHz

Sample	Added hydrogen (ppm)	R^2	Attenuation coefficient α (dB/cm)
N1	0	0.999	2.03 ± 0.20
N2	0	0.999	2.08 ± 0.21
N3	0	0.997	2.07 ± 0.21
H1	13.6 ± 0.7	0.999	$2{,}19 \pm 0.22$
H2	31.5 ± 1.4	0.999	2.19 ± 0.22
H3	60.5 ± 2.7	0.999	2.33 ± 0.23
H4	88.9 ± 4.0	0.999	2.24 ± 0.22
H5	107.0 ± 4.8	0.999	2.15 ± 0.22
H6	140.4 ± 6.3	0.999	2.11 ± 0.21
H7	170.6 ± 7.7	0.999	2.33 ± 0.23
H8	199.7 ± 9.0	0.999	2.31 ± 0.23
H9	304.5 ± 13.7	0.996	2.30 ± 0.23
H10	516.7 ± 23.3	0.999	2.41 ± 0.24

the exponential decay. From the analysis of R^2 it is possible to deduce that the exponential fitting of echoes at 10 MHz was excellent for eight of the samples and adequate for the rest of them. At 30 MHz the R^2 coefficients showed an excellent exponential fitting for all measurements. In this way, it can be asserted that spurious effects such as the non-parallelism of samples or diffraction losses were negligible for both.

The experimental attenuation (α) data at 10 MHz has been fitted as a function of hydrogen concentration by a logarithmic function:

$$\alpha\ (\mathrm{dB/cm}) = \alpha_0 + \alpha_1 \ln(C_{\mathrm{H}}\ (\mathrm{ppm})/C_0) \qquad (2)$$

where C_0 is the hydrogen concentration of the as-received material ($\cong$15 ppm), $\alpha_0 = 0.432 \pm 0.006$ and $\alpha_1 = 0.069 \pm 0.003$, with $R = 0.988$ and SD = 0.014. The experimental values and the regression line are displayed in Fig. 8. Conversely, the hydrogen concentration (C_{H}) may be calculated as function of the attenuation values by the exponential equation:

$$C_{\mathrm{H}} = C_0 \exp((\alpha - \alpha_0)/\alpha_1). \qquad (3)$$

The sensitivity of this method is greater for lower concentrations. By adding 100 ppm to the as-received material the attenuation increases 25%. Nevertheless, an error of 10% in the measured attenuation value produces an uncertainty in hydrogen concentration of 70%. So, the attenuation error had to be considerably reduced in order to obtain better accuracy.

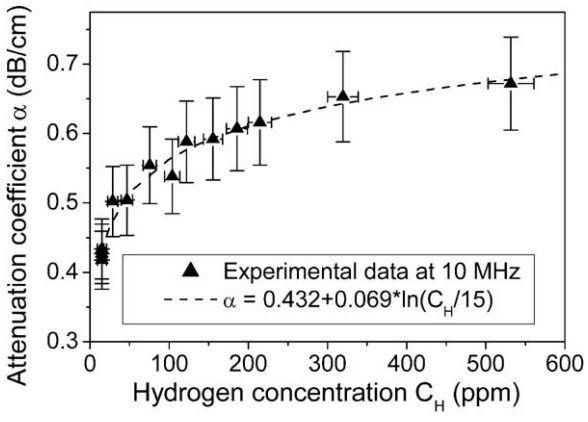

Fig. 8. Ultrasonic attenuation coefficient at 10 MHz versus hydrogen concentration.

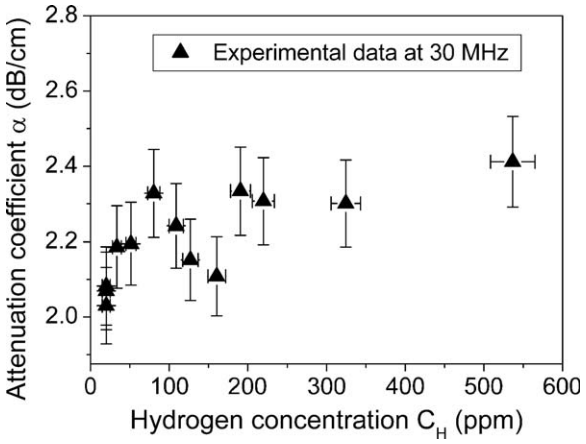

Fig. 9. Ultrasonic attenuation coefficient at 30 MHz versus hydrogen concentration.

The behavior for the attenuation coefficient versus the hydrogen level at 30 MHz (Fig. 9) is not monotonic, contrary to that observed with 10 MHz (Fig. 8). In this case the attenuation increases and decreases according to the added hydrogen quantity for each sample. The amplitude of the fluctuation shown in Fig. 9 exceeds the bar error. Therefore, this method cannot detect differences in hydrogen concentration quantity by means of attenuation coefficient measurement.

The attenuation values obtained in this work (for 10 and 30 MHz) and those from De et al. [10] (for 23 and 50 MHz) are replotted in Fig. 10. The quasi-monotonic logarithmic behavior of the values corresponding to 10 MHz are in good agreement with that obtained by De et al. at 23 MHz, with a difference in attenuation values caused by the higher frequency used in their measurements. For the highest frequencies instead, the behavior becomes fluctu-

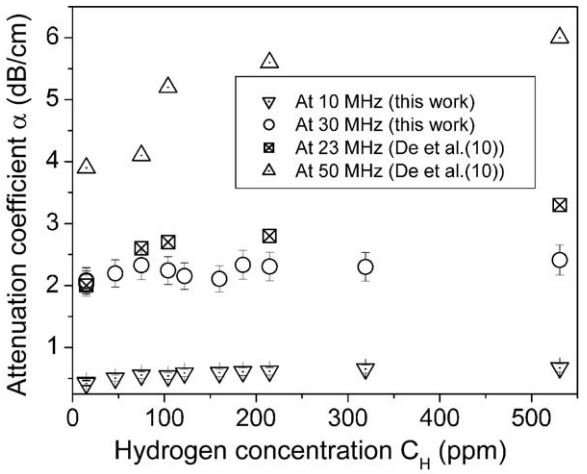

Fig. 10. Ultrasonic attenuation coefficient versus hydrogen concentration. Values measured in this work and those reported in [10], for different frequencies.

ating (in this paper at 30 MHz and De et al. with 50 MHz and 75 MHz).

Precipitation produces plastic deformation in both the matrix and the particle. The dislocations may contribute to the attenuation of ultrasonic waves. It would be necessary to apply a dislocation model to make quantitative predictions about the attenuation increase. Interfaces created between matrix and precipitated particles could be other attenuation sources, which cause a scattering process.

4. Conclusions

Ultrasonic velocity and attenuation were tested to measure hydrogen concentration in Zircaloy-4 with uniform hydride distribution. In the studied range (15–550 ppm), the propagation velocity of 10 MHz longitudinal waves versus Hydrogen concentration can be fitted by a linear regression (in spite of some fluctuations for concentration lower than 150 ppm). The constant error in velocity measurements and the smooth slope of the linear regression produced an error of 60 ppm in the hydrogen concentration prediction. Consequently this method is not recommended to evaluate hydrogen concentrations lower than 200 ppm, but it is worthwhile for higher hydrogen levels.

On the contrary, attenuation at 10 MHz is more sensitive to evaluate low hydrogen concentrations, because it increases with the logarithm of concentration. Nevertheless, it is necessary to reduce the error in attenuation measurements in order to enhance the precision of this method.

Attenuation at 30 MHz showed a fluctuating behavior with hydrogen concentration at low concentration. Hence, the attenuation measurement at this frequency is unable to detect differences in the added hydrogen concentration.

Acknowledgements

We wish to thank A. Acosta, R. Montero, R. Castillo Guerra, Dr M. Vicente Alvarez, N. Mingolo and C. di Grillo for technical assistance, Dr R. Piotrkowski, Dr M. Ipohorski and Dr D. Arias for useful discussion, Dr J. Ovejero García for his advice. This study has been supported by the Comisión Nacional de Energía Atómica (CNEA).

References

[1] C.E. Ells, C.E. Coleman, C.K. Chow, Can. Met. Quart. 24 (1985) 215.
[2] B. Cox, Mechanisms of hydrogen absorption by zirconium alloys, Atomic Energy Canada Limited, Report No. 8702, Chalk River, Ontario, 1985.
[3] F. Garzarolli, R. Manzel, S. Reschke, E. Tenkhoff, Review of corrosion and dimensional behavior of Zircaloy under water reactor conditions, in: Zirconium in the Nuclear Industry (Fourth Conference)ASTM STP, 681, American Society for Testing and Materials, Philadelphia, 1979, p. 91.
[4] C.E. Coleman, J.F.R. Ambler, Rev. Coating Corrosion 3 (1979) 105.
[5] M. Leger, G.D. Moan, A.C. Wallace, N.J. Watson, Growth fracture and nondestructive evaluation of hydride blisters in Zr–2.5 wt%Nb, in: L.F. Van Swam, C.M. Eucken (Eds.), Zirconium in the Nuclear Industry: Eight International Symposium, ASTM STP, 1023, American Society for Testing and Materials, Philadelphia, 1989, p. 50.
[6] A. Sawatzky, Can. Metall. Quart. 24 (1985) 227.
[7] E.G. Price, Overview of blister phenomena in relation to pressure tube integrity, in: E.G. Price (Ed.), The Formation and Characteristics of Hydride Blisters in c.w. Zircaloy-2 Pressure Tubes, AECL-11106, AECL, Ontario, 1994, p. 1.
[8] P. Efsing, K. Pettersson, Delayed hydride cracking in irradiated Zircaloy cladding, in: G.P. Sabol, G.D. Moan (Eds.), Zirconium in the Nuclear Industry: Twelfth International Symposium, ASTM STP 1354, American Society for Testing and Materials, West Conshohocken, PA, 2000, p. 340.
[9] M.P. Puls, Metall. Trans. 19 A (1988) 2247.
[10] P.K. De, J.T. John, S. Banergee, T. Jayakumar, M. Thavasimuthu, B. Raj, J. Nucl. Mater. 252 (1998) 43.
[11] G.F. Slattery, J. Inst. Metals 95 (1967) 43.
[12] A. Sawatzky, J. Nucl. Mater. 2 (1960) 62.
[13] R. Truell, C. Elbaum, B. Chick, Ultrasonic Methods in Solid State Physics, Academic Press, New York, 1969.
[14] E. Papadakis, J. Acoust. Soc. Am. 42 (1967) 1045.
[15] D. Hull, H. Kautz, A. Vary, Mater. Eval. 43 (1985) 1455.

[16] P.S. Addison, The Illustrated Wavelet Transform Handbook: Applications in Science, Engineering, Medicine and Finance, Institute of Physics Publishing, Bristol, 2002.
[17] L. Lanzani, M. Ruch, J. Nucl. Mater. 324 (2004) 165.
[18] A. Aladjem, Zirconium–hydrogen, in: F.A. Lewis, A. Aladjem (Eds.), Solid State Phenomena, Diffusion and Defect Data. B, 49-50, Cap. 7, Citec Publications Ltd., Zuerich, Switzerland, 1996, p. 281.
[19] R.L. Beck, W.M. Mueller, Zirconium hydrides and hafnium hydrides, in: W.M. Mueller, J.P. Blackledge, G.G. Libowitz (Eds.), Metal Hydrides, Academic Press, New York, USA, 1968, p. 241.
[20] S. Yamanaka, K. Yamada, K. Kurosaki, M. Uno, K. Takeda, H. Anada, T. Matsuda, S. Kobayashi, J. Alloys Comput. 293–295 (1999) 23.
[21] S. Yamanaka, K. Yamada, K. Kurosaki, M. Uno, K. Takeda, H. Anada, T. Matsuda, S. Kobayashi, J. Alloys Comput. 330–332 (2002) 99.
[22] T. Konishi, M. Honji, Texture effect of Zircaloy on ultrasonic velocity, in: D.G. Franklin, R.B. Adamson (Eds.), Zirconium in the Nuclear Industry: Sixth International Symposium, ASTM, STP, 824, American Society for Testing and Materials, Philadelphia, 1984, p. 256.